Journal of Magnetism and Magnetic Materials 471 (2019) 286–293

Contents lists available at ScienceDirect

Journal of Magnetism and Magnetic Materials

journal homepage: www.elsevier.com/locate/jmmm

Research articles

Microfluidic approaches for the production of monodisperse, superparamagnetic microspheres in the low micrometer size range

Reka Geczy[a,b], Monica Agnoletti[a,b], Mikkel F. Hansen[c], Jörg P. Kutter[a], Katayoun Saatchi[b], Urs O. Häfeli[a,b,*]

[a] Department of Pharmacy, Faculty of Health and Medical Sciences, University of Copenhagen, 2100 Copenhagen, Denmark
[b] Faculty of Pharmaceutical Sciences, University of British Columbia, Vancouver, British Columbia V6T 1Z3, Canada
[c] Department of Micro- and Nanotechnology, Technical University of Denmark, 2800 Kongens Lyngby, Denmark

ABSTRACT

The preparation of small, monodispersed magnetic microparticles through microfluidic approaches has been consistently challenging due to the high energy input needed for droplet break-off at such small diameters. In this work, we show the microfluidic production of 1–3 μm magnetic nanoparticle-loaded poly(D, L-lactide) (PLA) microspheres. We describe the use of two approaches, using a conventional flow-focusing microfluidic geometry. The first approach is the separation of target size satellite particles from the main droplets; the second approach is the direct production using high flow rate jetting regimes. The particles were produced using a polymeric thiol-ene microfluidic chip platform, which affords the straightforward production of multiple chip copies for single-time use, due to large feature sizes and replica molding approaches. Through the encapsulation of magnetite/maghemite nanoparticles, and their characterization with scanning electron microscopy (SEM) and vibrating sample magnetometry (VSM) measurements, we show that the resulting particles are monosized, highly spherical and exhibit superparamagnetic properties. The particle size regime and their magnetic response show potential for in vivo intravenous applications of magnetic targeting with maximum magnetic response, but without blocking an organ's capillaries.

1. Introduction

There are many potential *in vivo* applications for magnetic nanoparticles (MNPs) including therapeutic applications such as drug delivery (with the drug being encapsulated or bound to the MNPs) and magnetic hyperthermia (where the entire MNP heats up under the influence of an alternating magnetic field). Furthermore, diagnostic applications such as the imaging of receptor expression and cell types by magnetic particle imaging, MRI contrast and biosensing for diseases detection also benefit from MNPs [1]. For magnetic targeting under the influence of an external magnetic field, the typically used 20–100 nm sized particles are not ideal, as the magnetic force acting on a single particle is too small to overcome the blood stream's inertial and shear forces. Therefore, accumulation in the target tissues (e.g., a tumor) or a target organ (e.g., the pancreas) requires high magnetic fields and field gradients [2]. The easiest solution to overcoming these challenges in magnetic drug targeting is to increase the particle size, i.e., moving from nanoparticles to microparticles.

For *in vivo* intravenous administration, the magnetic microspheres (MMS) must be smaller than red blood cells, which have an average size of 6.5 μm, and should be spherical, monodisperse and superparamagnetic. Any capillary blockage can thus be avoided, both with and without an applied magnetic field, and allow for efficient and predictable magnetic targeting. An optimal targeting particle size might be one based on nature, namely the size of thrombocytes (blood platelets), which have a maximum size of between 2 and 3 μm [3], and typically circulate in the blood stream for 8–9 days [4]. This size regime effectively bypasses lung capillaries [5,6], while showing greater localization to the endothelium than the sub-micron counterparts [7]. Our lab favors the use of biodegradable monodisperse MMS, as they combine the defined magnetic targetability, the capability of encapsulation and controlled release of drugs with low toxicity, FDA-approval, and biodegradability once the MMS have done their job. Up to now, our lab made monodisperse MMS with a microfluidic glass chip at sizes between 8 and 50 μm [8], and later with a co-flow method to yield sizes up to 700 μm [9]. Smaller MMS had to be prepared by a solvent evaporation/extraction batch method, which yielded very broad size distributions between 1 and 2 μm [10].

The aim of the present study was to explore the production of small monodisperse MMS, which could be used in the bloodstream, would not clog the capillaries, and would be able to react to an external magnetic force. To ensure monodispersity and the continuous production of particles, microfluidic methods were utilized for the MMS production. We decided on investigating both direct and indirect microfluidic

* Corresponding author.
E-mail address: urs.hafeli@ubc.ca (U.O. Häfeli).

https://doi.org/10.1016/j.jmmm.2018.09.091
Received 29 June 2018; Received in revised form 23 September 2018; Accepted 23 September 2018
Available online 25 September 2018
0304-8853/

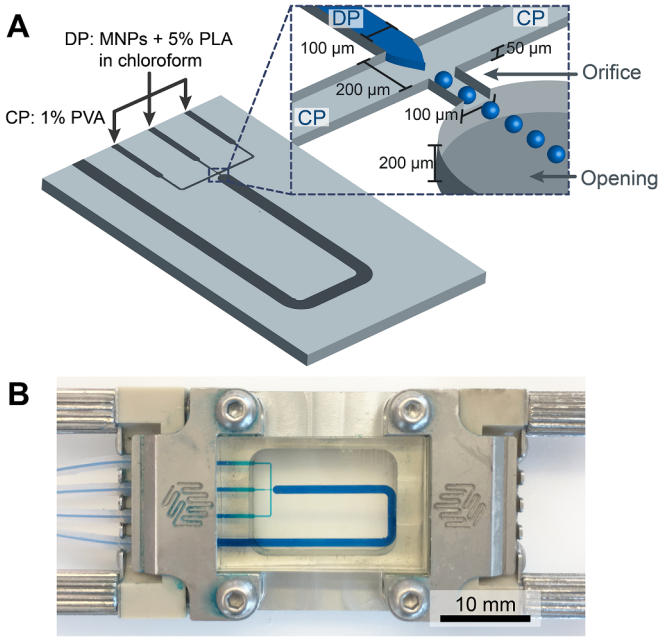

Fig. 1. Microfluidic chip and dimensions. A) Schematic illustration of flow focusing chip used for microsphere production. Chip dimensions include a 50 µm overall channel depth, a 100 µm wide and long orifice, and a 200 µm deep and 1 mm wide outlet opening. DP: dispersed phase, CP: continuous phase. B) Image of the thiol-ene chip within the chip holder. Chip dimensions are 22.5 × 15.0 × 4.0 mm.

methods to produce MMS sized in the low micrometer range (1–3 µm). The direct method utilizes flow focusing, where an inner non-miscible solvent stream breaks up into monosized droplets after passing through an orifice, as shown in Fig. 1. The indirect method refers to the collection of satellite particles that arise commonly in the just described microfluidic droplet generator in conjunction with the primary droplets.

Direct production of MMS of the size regime investigated here (~2 µm) has been realized by bulk methods [10], electrospray [11], and commercial flow focusing nozzles [12]. However, to our knowledge, a simple microfluidic chip has not yet been employed. This is partly because microfluidic production of small droplets is extremely difficult to achieve owing to the high energy input needed for droplet breakup. This generally requires small feature sizes as the production of droplets smaller than one-tenth of the orifice is rare [13], making the microfluidic chip fabrication costly and labor intensive. Indirect production of small MS through the collection of satellite droplets has been demonstrated [14–16], albeit for non-magnetic particles. Satellite particles are formed through the surface instabilities of the dispersed phase [17–19], and are generally considered problematic as the primary droplet polydispersity rapidly increases resulting in lower quality sample yield. However, if the aim is to produce small droplets using straightforward microfluidic techniques not requiring expensive fabrication approaches, then collection of satellite droplets may open an avenue towards obtaining the desired sized population.

In this study, we demonstrate the production and separation of satellite particles, as well as the direct production of 1 µm unloaded and 2 µm magnetite nanoparticle loaded PLA microspheres. Both methods were carried out using a simple-to-fabricate, polymeric microfluidic chip utilizing thiol-ene chemistry [20]. The microfluidic chip incorporates a flow focusing geometry with large feature sizes obtainable in most microfluidic laboratories without the use of a clean room. Our results show that the obtained MMS are narrow in size distribution, highly spherical, and superparamagnetic.

2. Materials and methods

2.1. Chip fabrication

Thiol-ene chips were fabricated as described previously in [21]. Chips were designed using a combination of Autodesk® Inventor® Professional (Autodesk Inc., San Rafael, CA, USA) and InventorCAM (SolidCAM Inc., Newtown, PA, USA). Computer numerical controlled (CNC) milling of the positive master mold (poly(methyl methacrylate) (PMMA) plates, Nordisk Plast A/S, Randers, Denmark) was executed by MiniMill (Minitech Machinery, Norcross, GA, USA), while the spacers and lids were CO_2 laser cut using an Epilog Laser Mini 18 (Golden, CO, USA). Combining the master mold, spacer, and lid, polydimethylsiloxane (PDMS, Sylgard® 184, Dow Corning, USA) negatives were molded and cured for 2 h at 80 °C, as recommended by the manufacturer. The following parameters for chip fabrication were obtained in a pilot experiment. Monomers were mixed 50% allyl excess with 1% Lucirin® TPO-L (BASF, Ludwigshafen, Germany) and molded within the PDMS negatives, using the thiol monomer (pentaerythritol tetrakis(3-mercaptopropionate) and tri-allyl monomer (1,3,5-triallyl-1,3,5-triazine-2,4,6(1H,3H,5H)-trione (both from Sigma Aldrich, Schnelldorf, Germany). Non-bonding sides of the molds were exposed to 1.6 s of UV light, 12 mW/cm^2 at 365 nm (LS-100-3C2 near UV light source, Bachur & Associates, Santa Clara, CA, USA), the cured halves were removed from the molds, and the chip was assembled by pressing together the two halves. Upon fabrication, the chips were washed and coated with an in-house synthesized, thiolated, hydroxyl-rich compound in order to reduce the contact angle from 70° to < 15°. The solution was prepared at 1.5% concentration with equal percentage of Irgacure 184 photoinitiator. Upon loading within the channels the chip was exposed to 12 mW/cm^2 (365 nm) UV light for 90 s. The coating procedure was repeated a total of 3 times. The final chip was cured for 10 min at 90 mW/cm^2 at 365 nm (Dymax 5000-EC Series UV curing flood lamp, Dymax Corp., Torrington, CT, USA).

2.2. Microsphere production

The dispersed phase (DP) consisted of poly(D, L-lactide) (PLA, 10–18 kDa, Resomer® R 202H, Sigma Aldrich, Schnelldorf, Germany) dissolved in chloroform at 2.5–5% (w/v) concentration (or 5% PLA and MNP's at 0.5–1% (w/v) mix). The continuous phase (CP) consisted of an aqueous solution of 1% (w/v) poly(vinyl alcohol) (PVA) (MW 30,000–70,000, 87–90% hydrolyzed, Sigma Alrich, Schnelldorf, Germany), 0.45 µm PTFE filtered prior to use. All solutions were prepared fresh prior to flow focusing. The flow focusing chip had an orifice of 50 µm deep, 100 µm wide and 100 µm long. The post-orifice opening was 1 mm wide and 200 µm deep to reduce potential interaction between the PLA droplets and channel walls (Fig. 1A). For satellite particle production, the microspheres were produced at Q_{DP} of 2 µL/min and Q_{CP} of 80 µL/min. For the continuous production of 1–3 µm microspheres, the flow rate was 1–2 µL/min for the DP while the CP was run at 600–2000 µL/min as indicated in the figures or figurelegends. Flow control was achieved by a neMESYS low-pressure syringe pump (CETONI GmbH, Korbußen, Germany) and glass syringes to minimize flow fluctuations often seen in traditional syringe pumps and plastic syringes. The chip was connected to the syringe pump using the Interface H and 4 Linear Connector 4-way system (Dolomite, Royston, UK). After collection, the particles were spun at 2000 rcf (5 min, at 4 °C) and resuspended in 100x volume of MilliQ water to facilitate solvent extraction.

2.3. Viscosity of and interfacial tension between the DP and CP solutions

To characterize and explain the mechanism of droplet formation, the dynamic viscosity of the DP (i.e., 5% PLA in chloroform) and the CP (i.e., 1% PVA in water) at the tested flow rates, and their interfacial

tension were measured. The dynamic viscosity was determined with an AR G2 Rheometer (TA Instrument, West Sussex, England) equipped with cone-plate measuring system (cone radius 40 mm, cone angle 1 degree) at 25 °C. All sample measurements were repeated 6 times. A rotational test was used to determine the shear solution viscosity (η, Pa·s) as a function of shear rate (γ, s^{-1}) from 0.1 to 1000 s^{-1} for the DP, and from 0.1 to 3000 s^{-1} for the CP. The viscosity values where taken at specific shear rates for both the DP and CP, which correspond to the shear rate (γ) values of the solutions in the opening chamber (the site of droplet break-off) at specific flow rates, according to the following equation:

$$\gamma = \frac{4 \cdot Q}{\pi \cdot r^3} \quad (1)$$

where Q is the flow rate (mL/s) and r is the radius of the opening (cm). The radius was estimated to match the cross-sectional area of the rectangular channels.

Interfacial tension was determined using the pendant drop method, where 5% PLA in chloroform was suspended in a solution of 1% PVA. Measurements were carried out on the KRUSS DSA100 drop shape analyzer (KRUSS GmbH, Hamburg, Germany). The PLA solution was slowly, drop-by-drop injected into a quartz container filled with PVA using a 500 µL glass syringe and an 18 gauge flat tip needle. Droplet shape and pinch-off was recorded on the camera and interfacial tension determined using the DSA100 software. Measurements were repeated > 20 times in order to understand the reproducibility of the measurements.

2.4. Fe_3O_4 nanoparticle synthesis

Magnetic iron oxide nanoparticles (MNP) were synthesized using the co-precipitation of Fe(II) and Fe(III) and coated with C_{12}-bisphosphonate as described previously by our group [9].

2.5. Imaging and size distribution

The samples were washed post-separation with 15 mL MilliQ water through centrifugation (2000 rcf, 5 min, at 4 °C) and resuspension. Light microscope images were taken on an Olympus IX71 inverted microscope. High-resolution surface mapping was done on a FEI Quanta 3D FEG scanning electron microscope at 2.0 kV acceleration voltage. Average diameters, standard deviation, and coefficient of variation were calculated by measuring at least 200 microspheres per sample using ImageJ. Gaussian fit for obtaining the histogram of distribution, and statistics were performed using GraphPad Prism.

2.6. Magnetization measurements

Vibrating sample magnetometry (VSM) measurements were carried out at room temperature in a LakeShore 7407 VSM. Each sample was prepared for measurements by (1) weighing a thin-walled 200 µL plastic tube, (2) adding the sample suspension and letting the liquid evaporate such that a sample pellet was formed at the bottom, (3) weighing the tube with the sample pellet, and (4) fixing the sample pellet using transparent nail polish. Measurements were performed using a custom-built sample mount in which the tube with the sample was mounted upside down. No corrections for background contributions were made. Results are reported as the specific magnetization (magnetic moment per sample mass), s, measured in units of Am^2/kg.

3. Results and discussion

3.1. Microfluidic material and design

For droplet generation, a polymeric microfluidic chip material was chosen due to its low cost and ease of production, while maintaining comparable results to glass. Naturally, due to the harsh chemical environment of chlorinated solvents used here, the polymer chips are not expected to last very long, but that is compensated for by the ease of replicate production when needed. The replicates are autoclavable, disposable, and eliminate the nuisances associated with clogging. Thiol-ene chips were used and were fabricated as we previously described [21], using CNC milling of PMMA plates, PDMS negative molding, and click-polymerization of thiol-ene monomers under UV light. The thiol-ene monomers were mixed in an off-stoichiometric ratio to gain allyl surface functional groups that are click-modifiable with thiol-containing compounds, e.g., to vary the surface properties to gain glass-like contact angles necessary for oil in water droplet formation [13]. To our knowledge, thiol-ene microfluidic chips are seldom used for oil in water

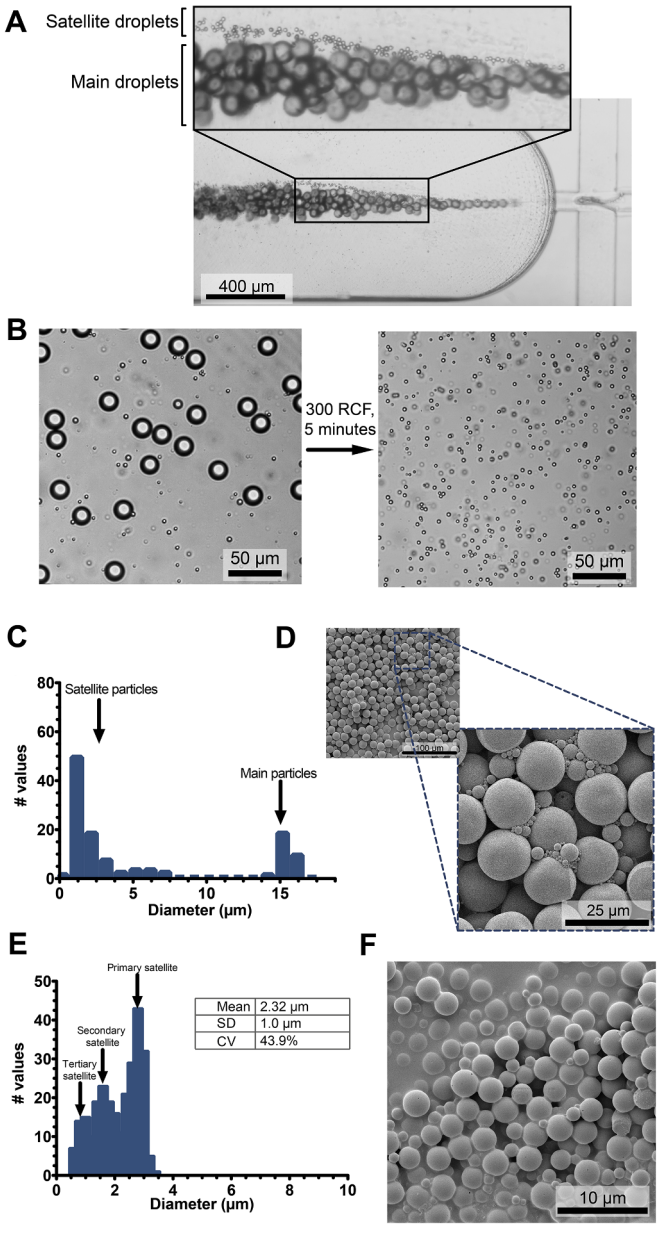

Fig. 2. Preparation, separation and characterization of satellite particles. A) Optical microscope image of the main and satellite droplets formed with 2 µL/min Q_{DP} and 80 µL/min Q_{CP}. Dispersed phase is 5% PLA in chloroform and continuous phase is 1% PVA. B) Light microscope image of PLA particles before (left) and after (right) centrifugation at 300 rcf for 5 min. C) Size distribution of particles based on the SEM images. D) SEM image of starting material showing the satellite particles. E) Size distribution of satellite particles based on the SEM images F) SEM image of satellite particles.

droplet production and have not been reported for the production of chloroform droplets for polymeric particle production. Thus far, only the production of ethylacetate [22] and toluene [23,24] droplets in water have been shown with these chip materials.

The chip geometry consisted of a flow focusing design where the dispersed phase (DP) flows perpendicularly to the continuous phase (CP), resulting in droplet break-off. The geometry includes a 100 µm wide and 50 µm deep orifice and a 1 mm wide and 200 µm deep outlet opening to minimize surface interaction between the channel walls and the PLA droplets (Fig. 1A). The final chip is optically transparent (Fig. 1B) and allows for continuous production of droplets for a few hours before severe swelling is induced by the chloroform exposure. As shown in the supplementary video files, the optical transparency also allows for observing the droplet formation directly on a microscope. This is particularly helpful to find stable production conditions (which generally take place within a couple of minutes).

3.2. Satellite particle approach

Droplet formation in a flow focusing system starts with the dispersed and continuous phase entering the junction/orifice and forming an interface where the continuous phase deforms the dispersed phase, creating an unstable thread that finally spontaneously breaks forming droplets [25]. During the production of the main droplets, additional breakup sequences of the thinned thread often results in the formation of satellite droplets [18]. The satellite droplets are generally very small, typically 1% in volume of the parent droplet [17], and thus present as an opportunity for small particle synthesis by separation and collection of the small satellites.

To achieve satellite formation, the flow rates and flow rate ratios in the so-called dripping regime were optimized to Q_{DP}:Q_{CP} of 2:80 µL/min (Fig. 2A, Supplementary Video 1). The video shows the formation of the satellite droplets in conjunction with the main droplet, where a small, single population is evident. The whole sample was collected, spun at 300 rcf in a centrifuge for 5 min, and the supernatant was retained. Here, the large PLA particles pelleted and the small particles remained in suspension; albeit, 40 ± 8% of the satellites were lost to the pellet. The supernatant contained only the small particles, allowing for rapid size-based separation of the sample Fig. 2B. Both the starting material and collected supernatant were further characterized using SEM. In Fig. 2C, the size distribution shows main particles of 15 µm diameter and a range of sub-7.5 µm satellite particles. The distribution was based on the SEM image shown in Fig. 2D, where both the main and satellite particles are clearly visible. After size separation, the remaining satellite particles are highly polydisperse, with primary, secondary and tertiary populations being evident, Fig. 2E. By light microscopy, such as in Supplementary Video 1, the large fraction of submicron particles are not visible. The clear distribution of secondary and tertiary satellites can only be observed using SEM, as seen in Fig. 2F. Nonetheless, the small particles are highly spherical in spite of a large range of diameters.

Our results of multiple satellite populations is consistent with previous studies [15,26]. Given the polydispersity, more focus needs to be directed towards the separation of each satellite species through both in-line and post-processing steps. Deterministic lateral displacement offers the finest resolution for size-based separation [14,26,27]; however, other methods such as Dean flow [28–30] and pinched flow fractionation [16] have also been employed. For the case of magnetic microspheres, active sorting through magnetic fields may offer a more efficient avenue for separation [31]. Furthermore, it is important to note that a single monodisperse population of satellite droplets has been reported through the modification of the flow focusing geometry, where droplet break-off is focused to a single point [32]. Finally, it may be worthy to consider the careful optimization of flow rates and ratios, as well as investigating the influence of the viscosity ratio between the two phases [33], the interfacial tension [34] and interfacial elasticity [35].

3.3. Jetting mediated synthesis of microspheres

A second approach for small particle formation is by increasing the continuous phase flow rate to the point where the feature sizes of the microfluidic chip (more specifically, around the orifice) no longer play a critical role in the resulting droplet size. Here, we investigated the upper flow rate and flow rate ratio limits of our microfluidic set-up in order to minimize the droplet size. The CP flow rate was systematically increased until the backpressure prevented any further increase and led to, e.g., mechanical issues with the syringe pump. Example flow profiles are shown in Fig. 3 and Supplementary Video 2, where a long, thin thread of the dispersed phase is visible, at the end of which jetting of the droplets occurs. The point of droplet break-off is dependent upon the CP flow rate and the flow rate ratio of the two phases. A significant increase in the outer phase flow rate, as tested here, changes the droplet formation regime, which can be characterized by the dimensionless capillary number (Ca), relating the influence of viscous *vs*. interfacial forces. The capillary number is often used in droplet microfluidics as a defining parameter for the regime of droplet formation. It is defined where η is the dynamic viscosity (Pa·s), U is the flow rate (m/s), and σ is the interfacial tension in (N/m). The Ca was calculated for both phases at the flow velocities corresponding to flow rates of 2 and 1800 µL/min in a 200 µm × 1000 µm opening by using our measured values of $\eta_{DP} = 2 \times 10^{-1}$ Pa·s for the DP, $\eta_{CP} = 6.3 \times 10^{-3}$ Pa·s for the CP and σ = 3 mN/m for the interfacial tension between the two phases.

The system can be defined by a Ca number of 1×10^{-2} for the DP and 0.11–0.33 for the CP. Comparing to a capillary number-based flow map shown in [36], the capillary numbers correspond to a regime that falls between jetting and threading. In this article, the authors define the threading regime as providing a stable thread with a length of 20*h*, with *h* being a characteristic length scale, namely the height of the square microfluidic channel in their experiments. In the jetting regime, on the other hand, droplets break off within the length of 20*h*. In our system, the length of the stable thread before droplet break-off was observed to be 10–20*h* depending on the Ca_{CP} or the flow rate of the CP. Here, *h* is defined as the hydraulic diameter, which is calculated from the side lengths of the rectangular channel cross section according to 2ab/(a + b), yielding a value of 333 µm. In this regime, droplet size is proportional to the diameter of the thread, where the end of the thread breaks off due to the amplifying Rayleigh-Plateau instability [25]. This means that the droplet diameter no longer relies on the microfluidic chip feature sizes but instead the flow rates, making the fabrication requirements much less stringent.

3.4. Empty PLA microsphere production

Initially, empty PLA particles were produced using the narrow jet regime. Stable jetting was observed from Q_{DP}:Q_{CP} of 2:600 µL/min up

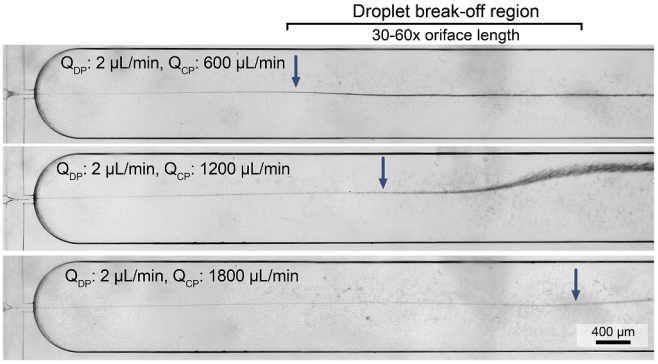

Fig. 3. High flow rate production of PLA droplets. Light microscope image of droplet formation at various flow rates and flow rate ratios (as indicated). Arrow shows approximate droplet break-off point.

to Q_{DP}:Q_{CP} of 2:1800 μL/min. For all flow rates investigated in this regime, the final PLA particle diameters remained under 2 μm with a narrow size distribution, having a coefficient of variation between 5 and 8%. At these flow rates, 150 mg of PLA microspheres are produced per day using a single chip; however, parallel production is a possibility for production upscaling. Size distribution and SEM images of the PLA particles produced at Q_{DP}:Q_{CP} of 2:1800 μL/min are shown in Fig. 4. For 2.5% PLA in chloroform, the average size is 1.16 μm with a coefficient of variation of 5.74%, as shown in Fig. 4A. The particles are highly uniform and spherical as seen in the SEM images (Fig. 4B and C). Increasing the PLA concentration to 5% resulted in slightly larger particles at 1.36 μm average in diameter, with a slightly better CV of 5.46% (Fig. 4D). Similarly, the SEM images show highly spherical and uniform particles (Fig. 4E and F).

3.5. Magnetic microsphere production

We previously showed the preparation of MNPs with a mixed magnetite/maghemite core and C_{12}-bisphosphonate coating having an average diameter of 12 ± 3.6 nm [9]. Approximately 0.5% or 1% (w/v) of homogeneously dispersed MNPs were added to the DP with 5% PLA in chloroform. Due to a different DP composition, the viscosity and interfacial tension changed which required the reoptimization of the flow rates for small MMS synthesis. In general, higher Reynolds numbers, but a smaller difference between the DP and CP flow rate ratios are required for effective MMS production. The final flow rates used were Q_{DP}:Q_{CP} of 2:1000 μL/min.

SEM shows a narrow size distribution for MMS with 0.5% or 1% (w/v) MNPs, albeit larger than the empty PLA microspheres. The larger size may be due to a combination of the modified flow rate condition as well as the effect of the MNP encapsulation. The 0.5% particles have a mean size of 2.08 ± 0.14 μm and a CV of 6.54% (Fig. 5A) with a smooth surface and spherical shape (Fig. 5B and C). The 1% particles are slightly larger at 2.31 ± 0.18 μm with a CV of 7.61% (Fig. 5D) and exhibit a more irregular and rougher surface (Fig. 5E and F). Such effects have been seen especially at higher concentrations, where dimples and sometimes even holes form, which are explained by jammed MNPs on the surface of the MMS. For a discussion of this effect, see [37].

Fig. 6A and B shows the assembly behavior of the particles in response to a magnet. Magnetization measurements were obtained for the starting MNPs (black) and the final MMS (blue and red), as shown in Fig. 6C. The magnetization curves confirm that the starting MNPs display non-negligible hysteresis, whereas the encapsulated MNPs show no detectable hysteresis. The hysteresis in the NP starting material is likely due to magnetic interactions between the particles in the dense sample. The lack of hysteresis in the MMS indicates that they are superparamagnetic at room temperature on a time scale of seconds. The specific magnetization of the 1% (w/v) sample is about 30% that of the starting NPs, while for the 0.5% (w/v) it is roughly 15%, showing good control over the magnetic loading into the PLA particles.

We demonstrated here that the production of 1–3 μm MMS is possible with microfluidic methods, at very narrow size distributions and without any hysteresis. To make these MMS appropriate for magnetic drug targeting, ideally higher MNP concentrations need to be incorporated. For large MMS, above 5 μm, we were in previous work able to incorporate up to about 50–60 wt% of magnetite [9,37]. Future work will optimize the MNP concentration, as well as maximize the magnetite to maghemite content in the MNPs, such as through the reduction of the coating thickness. The coating thickness of the MNPs with C_{12}-bisphosphonate is already thinner and more stable than a C_{18} oleic acid coating used by other authors [38]. We have previously attempted to further minimize its thickness to C_8, but the MNP behavior was not favorable, e.g. exhibiting unfavorable physiochemical properties, such as poor solubility in chloroform (results not shown).

4. Conclusion

In this work, we present two simple microfluidic methods for the production of 1–3 μm superparamagnetic particles. Both methods rely on easy-to-fabricate and cost-effective polymeric microfluidic chips with large feature sizes. Both of the methods presented here produce microspheres up to 6 mg/h. To increase throughput of microfluidic droplet generators, numerous studies have reported effective parallelization of the flow focusing junction on a single microfluidic chip, up to 512 identical junctions [39–41], resulting in mL/hour dispersed phase flow rates. Application of such parallelization, even if only 10-fold, could then result in more than 1 g microspheres per day, making it attractive for preclinical studies.

The microfluidic chip material, a thiol-ene polymer, offers the advantages of rapid production through replica molding and swift UV curing. Furthermore, the surface is click-modifiable, relatively heat resistant (allowing for sterilization), and disposable (for medical applications or in the event of clogging). Here, we demonstrate the utility of a material that is not normally compatible with chlorinated solvents being used for several hours of oil-in-water emulsion production. Thiol-ene chips have not been used before under such conditions for the production of polymeric particles. This opens an avenue for the rapid prototyping of channel geometries not easily achievable with glass due to time, effort and costs.

Initially, we show the production of small polymeric particles through the collection and separation of satellite particles. Even though our method yielded a broad range of satellite populations, starting from sub-micron to 2 μm in size, further strategies to minimize the number of satellites need to be investigated. Such include the modification of the outlet channel shape (Fig. 1A) from semi-circular to triangular, creating maximal velocity at a single point near the orifice resulting in more precise droplet generation [32]. Additionally, increasing the DP viscosity (through a higher concentration or molecular weight) should further aid in satellite population reduction [33]. Naturally, microfluidic size-based or magnetic separation is an alternative to achieving a single population of satellites [14,16,31]. All of these options are beyond the scope of this study, but utilizing the power of rapid prototyping through thiol-ene chips greatly facilitates the investigations of the channel geometries for both the production and separation of satellite particles.

Finally, we show the direct production of 1–3 μm polymeric particles without the need for particle separations. Importantly, this method allows for obtaining larger quantities of small microspheres, as opposed to the collection of satellites that only make up roughly 1% in volume of the sample [17]. Moreover, circumventing the use of satellites eliminates heavy losses of the starting material.

Using the direct production approach, we showed that the empty PLA particles are 1 μm in size, monodisperse, smooth and spherical. The MMS are 2 μm in size, similarly monodisperse, spherical and loaded with up to 30% MNPs, resulting in superparamagnetic properties. Here, the CP flow rate was increased to maximum velocities in order to form a long, thin thread, at the end of which jetting of the droplets occurs. In this droplet generation regime, the droplet size is proportional to the diameter of the thread, instead of the actual channel sizes. This results in extremely small droplet formation in a microfluidic chip with large feature sizes, circumventing the need for advanced clean room fabrication. While the particle size is mostly independent of the channel geometry in this regime, additional design changes may reveal further ways to reduce the particle diameters, such as, e.g., through the elongation of the orifice [42].

Overall, this work has exemplified the utility of polymeric chips for MMS production in harsh chemical environments. To the best of our knowledge, this is the first report to show production of MMS in this size regime and with well-defined distributions using a simple microfluidic set-up, thus clearly offering an alternative to more traditional fabrication approaches.

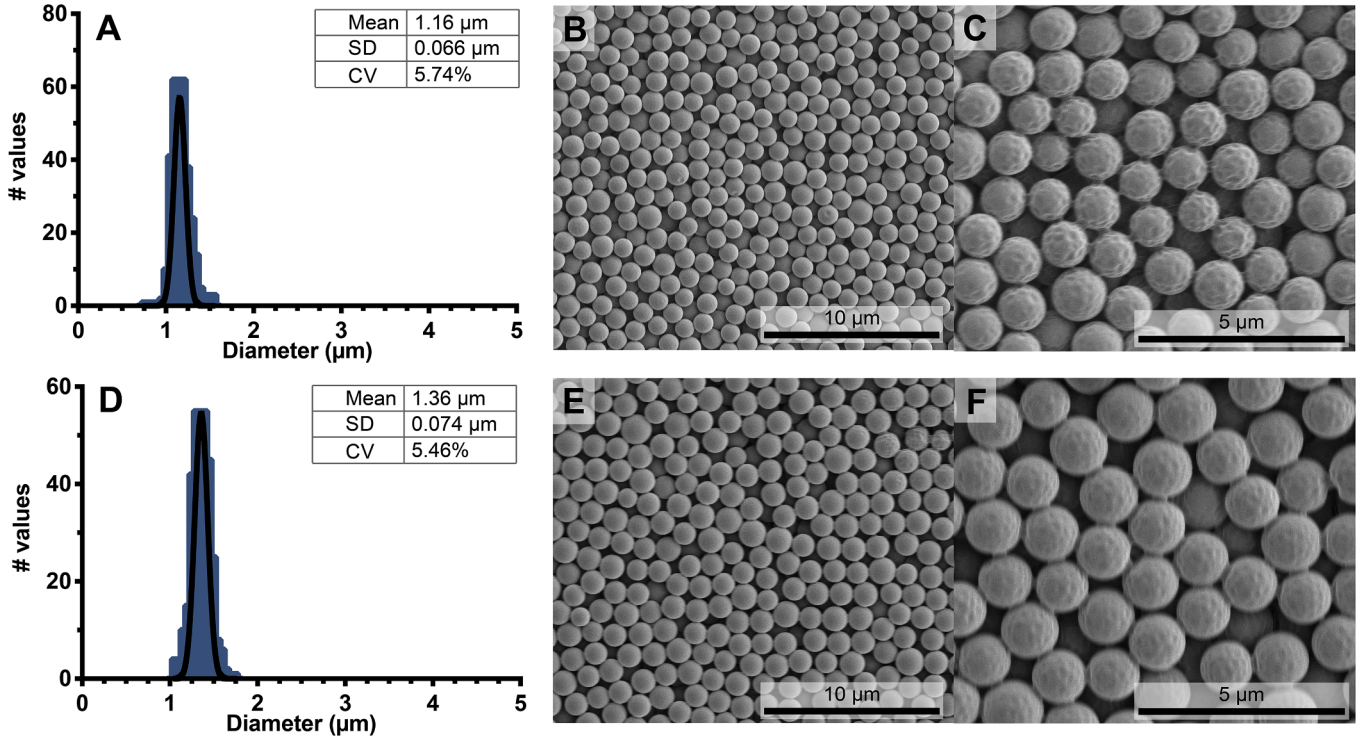

Fig. 4. Size distribution and surface mapping of empty PLA particles. A) Size distribution and statistics of MS made with 2.5% PLA in chloroform and shown in B) 15,000× magnification (SEM) and C) 50,000× magnification (SEM). D) Size distribution and statistics of MS made with 5% PLA in chloroform and shown in E) 15,000x magnification (SEM) and F) 50,000× magnification (SEM). Both samples produced at Q_{DP}:Q_{CP} of 2:1800 µL/min, diameters measured of > 200 particles for the histograms.

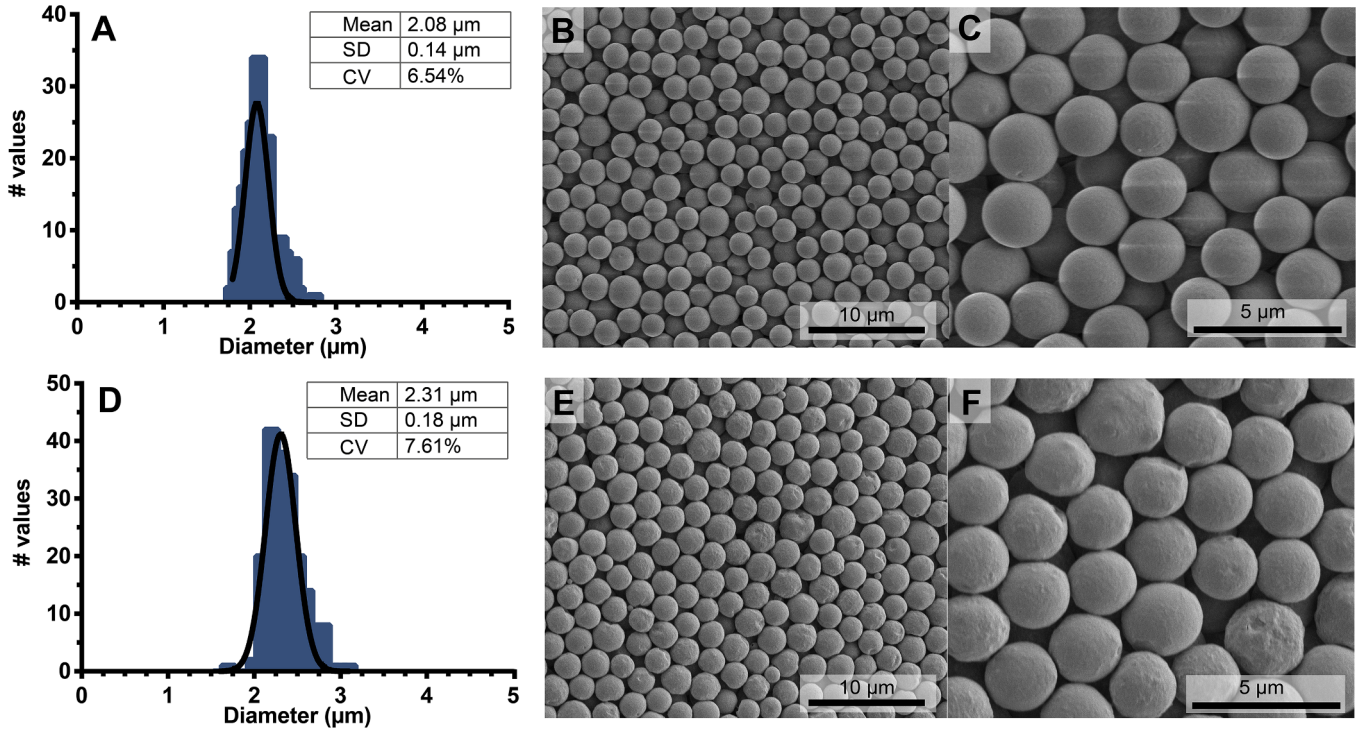

Fig. 5. Size distribution and surface mapping of MNP-loaded PLA particles. A) Size distribution and statistics of MMS made with 0.5% (w/v) magnetite and 5% PLA in chloroform and shown in B) at 15,000x magnification (SEM) and C) at 50,000x magnification. D) Size distribution and statistics of MMS made with 1% (w/v) magnetite and 5% PLA in chloroform and shown in E) at 15,000× magnification (SEM) and F) at 50,000x magnification. Both samples produced at Q_{DP}:Q_{CP} of 2:1000 µL/min, diameters of > 200 particles measured for the histograms.

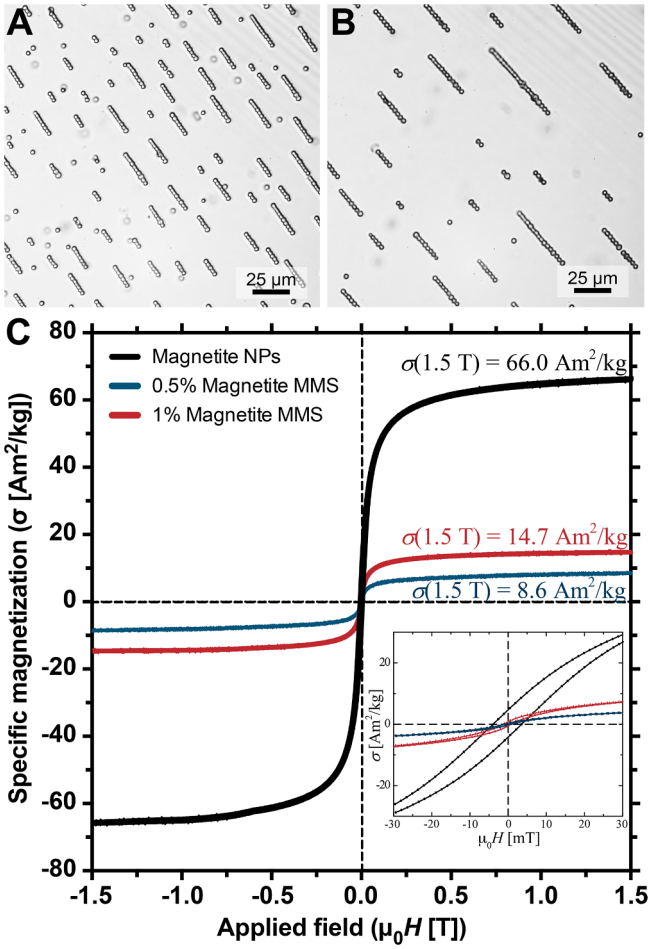

Fig. 6. Magnetic response and hysteresis curve. A) 0.5% or B) 1% (w/v) magnetite particles responding to a magnet imaged through light microscopy. C) Magnetization curve of starting MNPs (black), 0.5% MNP loaded MMS (blue), and 1% MNP loaded MMS (red). (For interpretation of the references to colour in this figure legend, the reader is referred to the web version of this article.)

Acknowledgments

We thank Cordula Grüttner and micromod Partikeltechnologie GmbH for providing the PLA. We acknowledge the Core Facility for Integrated Microscopy, Faculty of Health and Medical Sciences, University of Copenhagen for the SEM images. This study was supported by the Lundbeck Foundation, Denmark (grant number 2014-4176, the UBC-SUND Lundbeck Foundation professorship to UOH).

Appendix A. Supplementary data

Supplementary data associated with this article can be found, in the online version, at https://doi.org/10.1016/j.ijpharm.2018.05.006.

References

[1] K.M. Krishnan, Biomedical nanomagnetics: a spin through possibilities in imaging, diagnostics, and therapy, IEEE Trans. Magn. 46 (2010) 2523.
[2] A. Sarwar, A. Nemirovski, B. Shapiro, Optimal Halbach permanent magnet designs for maximally pulling and pushing nanoparticles, J. Magn. Magn. Mater. 324 (2012) 742.
[3] J.-M. Paulus, Platelet size in man, Blood 46 (1975) 321.
[4] D.W. Ross, L.H. Ayscue, J. Watson, S.A. Bentley, Stability of hematologic parameters in healthy subjects: intraindividual versus interindividual variation, Am. J. Clin. Pathol. 90 (1988) 262.
[5] J.D. Slack, M. Kanke, G.H. Simmons, P.P. Deluca, Acute hemodynamic effects and blood pool kinetics of polystyrene microspheres following intravenous administration, J. Pharm. Sci. 70 (1981) 660.
[6] M. Kanke, G.H. Simmons, D.L. Weiss, B.A. Bivins, P.P. Deluca, Clearance of 141Ce-labeled microspheres from blood and distribution in specific organs following intravenous and intraarterial administration in beagle dogs, J. Pharm. Sci. 69 (1980) 755.
[7] K. Namdee, A.J. Thompson, P. Charoenphol, O. Eniola-Adefeso, Margination propensity of vascular-targeted spheres from blood flow in a microfluidic model of human microvessels, Langmuir 29 (2013) 2530.
[8] U.O. Häfeli, K. Saatchi, P. Elischer, R. Misri, M. Bokharaei, N.R. Labiris, B. Stoeber, Lung perfusion imaging with monosized biodegradable microspheres, Biomacromolecules 11 (2010) 561.
[9] Z. Nosrati, N. Li, F.O. Michaud, S. Ranamukhaarachchi, S. Karagiozov, G. Soulez, S. Martel, K. Saatchi, U.O. Häfeli, Development of a coflowing device for the size-controlled preparation of magnetic-polymeric microspheres as embolization agents in magnetic resonance navigation technology, ACS Biomater. Sci. Eng. 4 (2018) 1092.
[10] H. Zhao, K. Saatchi, U.O. Häfeli, Preparation of biodegradable magnetic microspheres with poly (lactic acid)-coated magnetite, J. Magn. Magn. Mater. 321 (2009) 1356.
[11] S. Gun, M. Edirisinghe, E. Stride, Encapsulation of superparamagnetic iron oxide nanoparticles in poly-(lactide-co-glycolic acid) microspheres for biomedical applications, Mater. Sci. Eng. C 33 (2013) 3129.
[12] L. Martín-Banderas, R. González-Prieto, A. Rodríguez-Gil, M. Fernández-Arévalo, M. Flores-Mosquera, S. Chávez, A.M. Gañán-Calvo, Application of flow focusing to the break-up of a magnetite suspension jet for the production of paramagnetic microparticles, J. Nanomater. 2011 (2011) 4.
[13] G.F. Christopher, S.L. Anna, Microfluidic methods for generating continuous droplet streams, J. Phys. D Appl. Phys. 40 (2007) R319.
[14] N. Tottori, T. Nisisako, High-throughput production of satellite-free droplets through a parallelized microfluidic deterministic lateral displacement device, Sens. Actuators B 260 (2018) 918.
[15] Y.-C. Tan, A.P. Lee, Microfluidic separation of satellite droplets as the basis of a monodispersed micron and submicron emulsification system, Lab Chip 5 (2005) 1178.
[16] M. Yamada, M. Nakashima, M. Seki, Pinched flow fractionation: continuous size separation of particles utilizing a laminar flow profile in a pinched microchannel, Anal. Chem. 76 (2004) 5465.
[17] X. Zhang, Dynamics of drop formation in viscous flows, Chem. Eng. Sci. 54 (1999) 1759.
[18] M. Tjahjadi, H.A. Stone, J.M. Ottino, Satellite and subsatellite formation in capillary breakup, J. Fluid Mech. 243 (1992) 297.
[19] O. Carrier, E. Dervin, D. Funfschilling, H.-Z. Li, Formation of satellite droplets in flow-focusing junctions: volume and neck rupture, Microsyst. Technol. 21 (2015) 499.
[20] C.E. Hoyle, C.N. Bowman, Thiol–ene click chemistry, Angew. Chem. Int. Ed. 49 (2010) 1540.
[21] T.M. Sikanen, J.P. Lafleur, M.-E. Moilanen, G. Zhuang, T.G. Jensen, J.P. Kutter, Fabrication and bonding of thiol-ene-based microfluidic devices, J. Micromech. Microeng. 23 (2013) 037002.
[22] P. Wägli, A. Homsy, N.F. de Rooij, Norland optical adhesive (NOA81) microchannels with adjustable wetting behavior and high chemical resistance against a range of mid-infrared-transparent organic solvents, Sens. Actuators B 156 (2011) 994.
[23] L.-H. Hung, R. Lin, A.P. Lee, Rapid microfabrication of solvent-resistant biocompatible microfluidic devices, Lab Chip 8 (2008) 983.
[24] Z.T. Cygan, J.T. Cabral, K.L. Beers, E.J. Amis, Microfluidic platform for the generation of organic-phase microreactors, Langmuir 21 (2005) 3629.
[25] P. Zhu, L. Wang, Passive and active droplet generation with microfluidics: a review, Lab Chip 17 (2017) 34.
[26] N. Tottori, T. Hatsuzawa, T. Nisisako, Separation of main and satellite droplets in a deterministic lateral displacement microfluidic device, RSC Adv. 7 (2017) 35516.
[27] L.R. Huang, E.C. Cox, R.H. Austin, J.C. Sturm, Continuous particle separation through deterministic lateral displacement, Science 304 (2004) 987.
[28] A.A.S. Bhagat, S.S. Kuntaegowdanahalli, I. Papautsky, Continuous particle separation in spiral microchannels using dean flows and differential migration, Lab Chip 8 (2008) 1906.
[29] S. Dutz, M.E. Hayden, U.O. Häfeli, Fractionation of magnetic microspheres in a microfluidic spiral: interplay between magnetic and hydrodynamic forces, PLoS ONE 12 (2017) e0169919.
[30] S. Dutz, M.E. Hayden, A. Schaap, B. Stoeber, U.O. Häfeli, A microfluidic spiral for size-dependent fractionation of magnetic microspheres, J. Magn. Magn. Mater. 324 (2012) 3791.
[31] R. Zhou, C. Wang, Microfluidic separation of magnetic particles with soft magnetic microstructures, Microfluid. Nanofluid. 20 (2016) 48.
[32] Y.-C. Tan, V. Cristini, A.P. Lee, Monodispersed microfluidic droplet generation by shear focusing microfluidic device, Sens. Actuators B 114 (2006) 350.
[33] L. Derzsi, M. Kasprzyk, J.P. Plog, P. Garstecki, Flow focusing with viscoelastic liquids, Phys. Fluids 25 (2013) 092001.
[34] N.M. Kovalchuk, E. Nowak, M.J.H. Simmons, Effect of soluble surfactants on the kinetics of thinning of liquid bridges during drops formation and on size of satellite droplets, Langmuir 32 (2016) 5069.
[35] C.X. Zhao, E. Miller, J.J. Cooper-White, A.P.J. Middelberg, Effects of fluid–fluid interfacial elasticity on droplet formation in microfluidic devices, AIChE J. 57 (2011) 1669.
[36] T. Cubaud, T.G. Mason, Capillary threads and viscous droplets in square microchannels, Phys. Fluids 20 (2008) 053302.

[37] M. Bokharaei, T. Schneider, S. Dutz, R.C. Stone, O.T. Mefford, U.O. Häfeli, Production of monodispersed magnetic polymeric microspheres in a microfluidic chip and 3D simulation, Microfluid. Nanofluid. 20 (2016) 6.
[38] X. Liu, M.D. Kaminski, J.S. Riffle, H. Chen, M. Torno, M.R. Finck, L. Taylor, A.J. Rosengart, Preparation and characterization of biodegradable magnetic carriers by single emulsion-solvent evaporation, J. Magn. Magn. Mater. 311 (2007) 84.
[39] M.K. Mulligan, J.P. Rothstein, Scale-up and control of droplet production in coupled microfluidic flow-focusing geometries, Microfluid. Nanofluid. 13 (2012) 65.
[40] D. Conchouso, D. Castro, S.A. Khan, I.G. Foulds, Three-dimensional parallelization of microfluidic droplet generators for a litre per hour volume production of single emulsions, Lab Chip 14 (2014) 3011.
[41] E. Amstad, M. Chemama, M. Eggersdorfer, L.R. Arriaga, M.P. Brenner, D.A. Weitz, Robust scalable high throughput production of monodisperse drops, Lab Chip 16 (2016) 4163.
[42] L. Wu, X. Liu, Y. Zhao, Y. Chen, Role of local geometry on droplet formation in axisymmetric microfluidics, Chem. Eng. Sci. 163 (2017) 56.